Desalination and Water Treatment
www.deswater.com

doi: 10.5004/dwt.2018.22290

113 (2018) 213–226
May

Cadmium(II) and lead(II) removal from aqueous solutions by heat-treated Algerian halloysite

Samir Kadi[a,*], Salima Lellou[a], Kheira Marouf-Khelifa[b], Jacques Schott[c], Amine Khelifa[b]

[a]*Laboratoire de Physiologie Végétale Appliquée au Culture Hors Sol, Département des Sciences de la Nature et de la Vie, Université Ibn Khaldoun Tiaret BP 78 Zaaroura, Tiaret 14000, Algeria, Tel. +213 7 78 25 46 16, Fax +213 45 21 10 18, email: ksam792002@yahoo.fr (S. Kadi)*
[b]*Laboratoire de Structure, Elaboration et Applications des Matériaux Moléculaires (S.E.A.2M.), Département de Génie des Procédés, Université de Mostaganem, Mostaganem 27000, Algeria, email: kheira_marouf@yahoo.fr (K. Marouf-Khelifa), aminekhelifadz@yahoo.fr (A. Khelifa)*
[c]*Laboratoire Géosciences Environnement Toulouse (GET), CNRS-IRD-OMP-Université de Toulouse, 14, Avenue Edouard Belin, 31400 Toulouse, France, email: jacques.schott@get.omp.eu (J. Schott)*

Received 8 July 2017; Accepted 1 April 2018

ABSTRACT

The removal of cadmium(II) and lead(II) from aqueous solution was investigated using thermally processed halloysite. The samples were previously heated in the 200–1000°C range at interval of 200°C. The resulting materials were characterized by thermal analysis, electron microscopy, X-ray diffraction, electrophoretic mobility measurement, and N2 adsorption. Metal adsorption was studied as a function of pH, contact time, temperature, metal and adsorbent concentrations, and correlated with the physicochemical properties of the materials. A particular interest has been focused on the spectroscopic study to elucidate the mechanism of the interaction of M^{2+} (M = Cd or Pb) cations with the best adsorbent. The kinetic and equilibrium data were adequately described by the pseudo-second order and Redlich–Peterson models, respectively. The mechanism mainly involved an electrostatic interaction between these metallic cations and the hydroxyl groups of surface. Whatever metal, maximum adsorption occurred for the material that preserved its structure, i.e. H200 (halloysite heated at 200°C) for Pb(II) and H400 for Cd(II). The intermediate adsorption of H600 and H800 was explained by their poorly organized structures due to dehydroxylation. H1000 was found to be the worst adsorbent due to its low specific surface area. Regardless of the material, the adsorption sequence was: Pb > Cd, which was correlated with the ionic properties of each metal. As long as it preserves its structure, halloysite clay proves to be an efficient adsorbent for removing heavy metals from aqueous solutions.

Keywords: Halloysite; Thermal treatment; Characterization; Adsorption; Cd(II); Pb(II)

1. Introduction

Cd(II) and Pb(II) are used in several industries, such as metallurgical alloys, electroplating, photography, pigmentation, paint, manufacture of battery and munition, and petroleum refining [1]. After use, these metal ions are mostly released into effluents. Their toxicity is enhanced by a biomagnification in the food chain and an accumulation in living tissues [2]. Cadmium intoxication leads to lung, liver and kidney damage, bone lesions, cancer and hypertension [3]. The presence of lead in the human body causes enormous health problems (headaches, abdominal pain, visual disturbances ...) that can lead to anemia or paralysis or even death in children [4]. Among the numerous methods available for removing heavy metals may be mentioned chemical precipitation, ion exchange, electrochemical treatment, reverse osmosis, and adsorption. Chemical precipitation is not suitable for removing low concentrations and also produces a large amount of sludge. Ion exchange is expensive and sophisticated. Electrolytic processes are considered to be cost-effective only for more concentrated solutions. Reverse osmosis, although very effective, is a

*Corresponding author.

high-cost process because the membranes require a frequent replacement [5]. Adsorption was found to be an effective, economical, and easy technique to implement. Its other advantages are applicability at very low concentrations, suitability for using batch and continuous processes, little sludge generation, and possibility of regeneration and reuse.

Different adsorbents were used to fix Cd(II) and/or Pb(II) from aqueous solution, such as organic membrane [6], nanocomposites [7], sawdust [8], activated carbon [9], and polymer [10]. These materials were found to be costly in addition to disadvantages due to their subsequent treatment and regeneration. Among the inexpensive and readily available materials, 2:1 type layered clays have been extensively studied [11–13]. In contrast, 1:1-type minerals such as halloysite have been little investigated.

The originality of this manuscript was to investigate the possibility of using Algerian halloysite heated in the 200–1000°C range as adsorbent of lead and cadmium from aqueous solutions. A particular interest has been focused on the spectroscopic study to elucidate the mechanism of the interaction of M^{2+} (M = Cd or Pb) cations with the best adsorbent. Before adsorption, the materials were characterized by TG/DTA, TEM, XRD, electrophoretic mobility measurement, and N_2 adsorption. Metal adsorption was studied as a function of adsorbent concentration, pH, contact time, metal concentration, and temperature. The resulting parameters were correlated with the physicochemical properties of the materials.

2. Materials and methods

2.1. Materials

Halloysite from Djebel Debbagh, Guelma (eastern region of Algeria) was ground, ultrasonically dispersed in deionized water and dried, after separation by filtration. Its characteristics were reported in a previous work [14]. Samples were heated in a muffle furnace at 200, 400, 600, 800, and 1000°C, at a rate of 10°C min^{-1}. Each sample was processed at the relevant temperature for 2 h. It is well-known that 2 h is a sufficient time that induces some transformations for different materials [15,16]. The samples were named H, H200, H400, H600, H800, and H1000.

2.2. Characterization

Thermal analysis (TG-DTA) was performed on a Netzsch Sta 409 C instruments. Approximately 190 mg of halloysite was heated in an alumina crucible with a heating rate of 17°C min^{-1}, under an atmosphere of high purity N_2. TEM images were determined with a Jeol 2100 electron microscope. An EDX detector for X-ray energy dispersive was attached to this microscope. The clay sample was previously ultrasonically dispersed in ethanol for 5 min. X-ray powder diffraction patterns were obtained using a Philips PW 1830 diffractometer with CoKα radiation (λ = 0.1789 nm) operating at 40 kV and 25 mA. XRD data were collected over a 2θ range of 5–90° with a step width of 0.03°. A Zetacad (CAD Inst., France) zeta-meter, equipped with microprocessor unit, was used for streaming potential measurements. The unit automatically calculates the electrophoretic mobility of particles. The assessment of textural properties was carried out by nitrogen adsorption–desorption. The measurements were performed at 77 K via a Tristar instrument (Micromeritics). Specific surface areas were determined by the BET method. External surface areas and micropore volumes were calculated by the *t*-plot method. Mesopore volume was assessed from the desorption branch.

2.3. Adsorption procedure

Stock solutions of cadmium(II) or lead(II), of concentration 200 mg L^{-1}, were prepared by dissolving an appropriate amount of nitrate salts [$Cd(NO_3)_2{\cdot}4H_2O$ or $Pb(NO_3)_2$] in distilled water. The working solutions were prepared by diluting the stock solution into the desired concentrations. The adsorption experiments were performed via the batch method. 0.04 g of the halloysite clay were mixed with 20 mL of metallic cation solution. After each experiment, the solution was separated by filtration. The filtrate was analyzed by flame atomic absorption spectrophotometry (FAAS), using a Perkin-Elmer 400 series spectrophotometer. The adsorbed amount was calculated from the difference between the initial and final concentrations. The effects of metal and adsorbent concentrations, pH, contact time, and temperature were studied. The experimental conditions are outlined in Table 1.

2.4. Theoretical background

2.4.1. Adsorption kinetics

The kinetic data were described with pseudo-first-order, pseudo-second-order, and intraparticle diffusion models, which are presented, respectively, as follows [17–19]:

Table 1
Experimental conditions during the adsorption of Cd(II) and Pb(II)

Adsorbent concentration	Clay 2, 4, 6, 8, and 10 g L^{-1} Temperature 298 K, contact time 2 h
pH	pH Pb(II) 2.0, 3.5, 5, and 6
	pH Cd(II) 2.0, 3.5, 5, 6.5, and 8
	Clay 2 g L^{-1}, temperature 298 K, contact time 2 h
Kinetics	Contact time 1, 3, 5, 10, 20, 40, 60, 120, and 240 min
	Clay 2 g L^{-1}, temperature 298 K, pH(Pb^{2+}) 6.5, pH(Cd^{2+}) 6.0
Isotherms	Pb(II) 10, 20, 40, 60, 100, and 200 mg L^{-1}. Clay 2 g L^{-1}, temperature 298 K, contact time 2 h, pH 6.5
	Cd(II) 10, 20, 40, 60, 100, and 200 mg L^{-1}. Clay 2 g L^{-1}, temperature 298 K, contact time 2 h, pH 6.0
Temperature	Temperature 298, 313, and 328 K. Clay 2 g L^{-1}, Pb(II) 10, 20, 40, 60, 100, and 200 mg L^{-1}, contact time 2 h, pH 6.5.
	Cd(II) 10, 20, 40, 60, 100, and 200 mg L^{-1}, contact time 2 h, pH 6.0

$$log\left(Q_e - Q_t\right) = log\, Q_e - \left(K_1.t/2,303\right) \quad (1)$$

$$t/Q_t = \left(1/K_2 Q_e^2\right) + t/Q_e \quad (2)$$

When $t \to 0$, the initial adsorption rate, h (mg g^{-1} min^{-1}), is defined as:

$$h = K_2.\, Q_e^2 \quad (3)$$

$$Q_t = K_{id}.\, t^{1/2} + C \quad (4)$$

where Q_e: amount adsorbed at equilibrium (mg g^{-1}), Q_t: amount adsorbed at time t (mg g^{-1}), K_1: pseudo-first-order rate constant (min^{-1}), t: contact time (min), K_2: pseudo-second-order rate constant (g mg^{-1} min^{-1}), K_{id}: intraparticle diffusion rate constant (mg g^{-1} min$^{-1/2}$), and C: constant proportional to the boundary layer thickness.

2.4.2. Adsorption equilibrium

The equilibrium data were analyzed by Langmuir, Freundlich, and Redlich–Peterson isotherm models, which are presented, respectively, as follows [20–22]:

$$Q_e = Q_m \frac{K_L C_e}{1 + K_L C_e} \quad (5)$$

$$Q_e = K_F C_e^{\frac{1}{n}} \quad (6)$$

$$Q_e = \frac{K_{RP} C_e M}{1 + (K_{RP} C_e)^{\beta}} \quad (7)$$

where: C_e equilibrium concentration (mg L^{-1}), Q_e: amount adsorbed at equilibrium (mg g^{-1}), K_L: Langmuir adsorption constant (L mg^{-1}), Q_m: maximum adsorption capacity (mg g^{-1}), K_F: Freundlich adsorption constant (L g^{-1}), n: constant related to adsorption intensity, K_{RP} and M: Redlich–Peterson constants, and β: heterogeneity factor that depends on the surface properties of adsorbent.

2.4.3. Adsorption thermodynamics

The thermodynamic parameters ΔH^0, ΔS^0, and ΔG^0 were evaluated using the following equations:

$$ln\, K_d = \left(-\Delta H^0/R.T\right) + \left(\Delta S^0/R\right) \quad (8)$$

$$K_d = Q_e/C_e \quad (9)$$

$$\Delta G^0 = \Delta H^0 - T\Delta S^0 \quad (10)$$

where ΔH^0, ΔS^0, and ΔG^0 are the changes in enthalpy (kJ mol^{-1}), entropy (J mol^{-1} K^{-1}), and Gibbs energy (kJ mol^{-1}), respectively, T: absolute temperature (K), R: gas constant (J mol^{-1} K^{-1}), and K_d: distribution coefficient (L g^{-1}).

3. Results and discussion

3.1. Characterization

3.1.1. Thermal analysis

DTA and TG curves are depicted in Fig. 1. The DTA curve shows that the decomposition process of Algerian halloysite takes place in three main steps: (i) a first endothermic peak in the range 50–240°C, corresponding to the release of water adsorbed on the surface of particles, (ii) a second endothermic peak between 480 and 640°C, due to structural decomposition. The peak centered at 580°C is assigned to the dehydroxylation of structural aluminol groups [23], and (iii) an exothermic peak at 993°C, caused by the formation of amorphous SiO_2 and γ-Al_2O_3 [24]. The thermogravimetric curve highlights a continual mass loss between 25 and 1100°C of 12.5%. In the dehydroxylation range, a steep slope was obtained, corresponding to a major weight loss of 6.7% between 400 and 700°C. The dehydroxylation of halloysite consists in the following reaction:

$$Al_2O_3\ 2SiO_2\ 2H_2O \xrightarrow{\text{dehydroxylation}} Al_2O_3\ 2SiO_2 + 2H_2O \quad (11)$$

3.1.2. Transmission electron microscopy

TEM images of untreated halloysite (H), H600, and H1000 are presented in Fig. 2. The particles of the starting material evidences a cylindrical shape whose the transparent central area runs longitudinally along the cylinder, indicating a hollow and open-ended structure. Particles differ both in diameter and length. Their external diameters vary from 50 to more than 100 nm, while the internal diameter is ca. 10 nm. These rolled tubes consist in a number of aluminosilicate sheets, curved, and closely packed. One finds 2 layer distances, one of 7.2 and another of 4.4 Å corresponding to the (001) and (111) reflections,

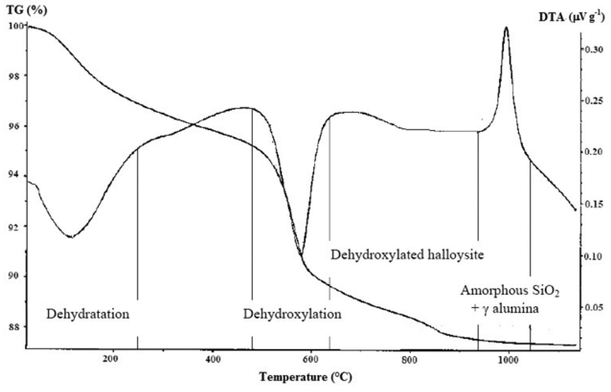

Fig. 1. DTA and TG curves for untreated halloysite.

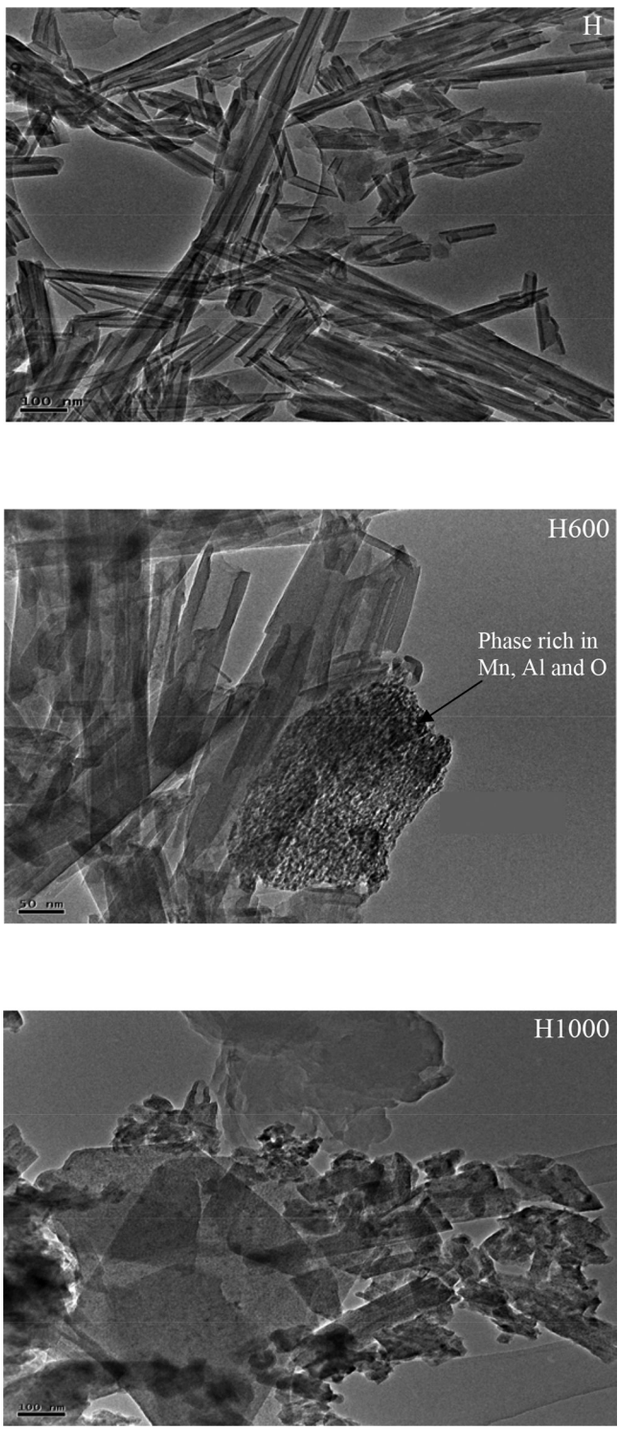

Fig. 2. Transmission electron microscopy images of the halloysite solids.

respectively. Nanotubular particles were also obtained for H600, proving that the heat treatment at 600°C maintains the morphology of halloysite. Their external and internal diameters vary from 30 to 180 nm, and from 10 to 30 nm, respectively. A phase rich in Al, O, and Mn was evidenced by EDX. This phase consists of agglomerated small plates of diameter ca. 10 nm. Interlayer spacing could not be highlighted. This is probably due to the fact that the layers are immediately destroyed under the beam of electrons. H1000 presents both tubular and plate morphologies. The nanotubes are damaged. Their external diameters are ca. 70 nm. At 1000°C, the dehydroxylation phenomenon alters the morphology of halloysite clays, because it leads to the formation of γ-Al_2O_3 and amorphous SiO_2.

3.1.3. XRD analysis

XRD patterns of unheated and halloysites heated at 200, 400, 600, 800, and 1000°C are depicted in Fig. S1 in the supplementary data. The diffractogtam of the starting material shows a basal reflection at 7.6 Å (2θ = 13.5°) with a shoulder at 10 Å (hh) (2θ = 10.3°), indicating a partially hydrated halloysite. A feature of the X-ray pattern of halloysite having common tubular morphology is the very intense reflection at ~4.4 Å. The X-ray diagram of Algerian halloysite shows a prominent reflection at 2θ value of 23.5°, corresponding to d-spacing of 4.4 Å. Quartz (*q*) and calcite (*c*) reflections were also observed. Their low intensities indicate minor quantities. The thermal treatment at 200 and 400°C does not cause significant changes of structure, except that the intensity of the peaks characteristic of halloysite increases for H200 and H400. This increase may be ascribed to that of halloysite content in the sample, after removing physisorbed water. This shows that the crystalline structure of halloysite is stable up to 400°C. For the solids treated at 600 and 800°C, no clear diffraction peak is observed. This indicates a poorly organized structure and a progressive amorphisation of structure, which is due to the structure –OH group breakage. For H1000, a recrystallization process arises from amorphous substance, materialized by the appearance of several reflections, and identified as due to γ-Al_2O_3. In parallel, the broad band observed in the 2θ range of 5–18° is probably due to amorphous SiO_2. In other words, the structural rearrangement of dehydroxylated halloysite results in the formation of γ-Al_2O_3 and amorphous SiO_2.

3.1.4. Electrophoretic mobility

Electrokinetic properties play a significant role in understanding the adsorption mechanism of inorganic species at the solid/solution interface. Fig. 3 shows the changes of the electrophoretic mobility of halloysitic clays as a function of pH. Untreated halloysite has an isoelectric point (I.E.P.) of 2.5 [14], corresponding to a surface charge neutralized. The heat treatment in the range 200-800°C slightly modifies this value within a narrow range of 2.6 ± 1. The measured values of mobility are also in close agreement, i.e., between 4 and -9×10^{-8} $m^2{\cdot}V^{-1}{\cdot}S^{-1}$. The increase of suspension pH from I.E.P. results in an increase in the negative charge of halloysitic clay. This can be ascribed to either the adsorption of OH^- ions onto the positive charge centers or the deprotonation of surface hydroxyl groups [25]. H1000 behaves differently in comparison with the other samples. Its mobility varies considerably with pH, from 26 to -120×10^{-8} $m^2{\cdot}V^{-1}{\cdot}S^{-1}$,

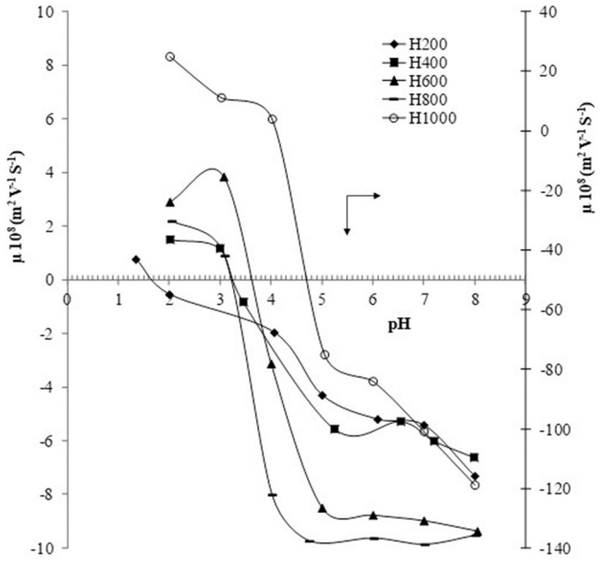

Fig. 3. Electrophoretic mobility of the halloysite solids.

whereas the neutralization of its surface charge occurs at a pH of 4.7. This behavior could be explained by the formation of γ-Al_2O_3 and amorphous silica. A literature review shows that alumina has an I.E.P. of 7.8, while that of silica is 1.8 [26].

3.1.5. Textural analysis

The textural parameters are summarized in Table 2. S_{BET} remain fairly constant up to 800°C, beyond which it drastically decreased from 63 m^2/g for H200 to 17.8 m^2/g for H1000. Whatever the sample, the values of external surface are higher than those of internal surface, while the volumes of micropores are negligible. Total volume is mainly represented by mesopores. They represent up to 99% of total volume for H800. The lowest value of total volume of pores was found for H1000. The solid obtained at 1000°C consists of grains of alumina and amorphous silica. The latter precipitates into the matrix and fills pores, resulting in a smaller specific surface area [27].

3.2. Adsorption of Cd(II) and Pb(II)

3.2.1. Effect of adsorbent concentration

To evaluate the optimum dosage of the solids, different adsorbent concentrations were used (Fig. 4). Metal uptake decreases with increasing concentration. This evolution may be caused by an unsaturation of adsorption sites, and/or an aggregation of the adsorbent particles, resulting in a decrease in the total surface area and an increase in diffusional path length [28]. This result was previously reported for Cd(II) and Cr(VI) adsorption by modified kaolinites [5]. Optimum obtained for a concentration of 2 g L^{-1} was considered in the subsequent experiments.

3.2.2. Effect of pH

To prevent metal precipitation, the adsorption of Cd(II) and Pb(II) ions was studied over the pH range 2–6 and 2–8, respectively. The effect of pH is shown in Fig. 5 at $C_{initial} = 80$ mg L^{-1}. As illustrated in Fig. 5, the removal of Cd(II) and Pb(II) from aqueous solution is pH-dependent. The adsorption capacity of Pb^{2+} increases with increasing solution pH. Such an evolution was also obtained for Cu(II) adsorption by halloysites intercalated with sodium acetate [29]. We cannot exceed pH 6 to avoid the hydrolyzed lead species such as $Pb(OH)^+$ and $Pb(OH)_2$ [30]. The uptake of Cd(II) first increases with pH and then reaches a plateau around 6.5. The same trend was observed for Cd^{2+} adsorption by different materials [31]. At low pH, adsorption is insignificant and can be explained by the fact that electrostatic repulsion occurs between M^{2+} ions (M^{2+} = Cd^{2+} or Pb^{2+}) and the positively charged edge groups (S-OH_2^+) [32]:

$$-SO + H-OH \xrightarrow{H^+} S-OH_2^+ + OH^- \quad (12)$$

When pH increases, clay surface becomes negatively charged favoring M(II) uptake:

$$-SOH + OH^- \rightleftarrows -SO^- + H_2O \quad (13)$$

$$-SO^- + M^{2+} \rightleftarrows -S-O\ldots M^{2+} \quad (14)$$

With increasing pH, high removal efficiency can be attributed to electrostatic interactions between the

Table 2
Textural parameters of the halloysite solids

Samples	Specific surface area SBET (m^2/g)	External surface area Sext (m^2/g)	Internal surface area Sint (m^2/g)	Total volume of pores (cm^3/g)	Micropores volume (cm^3/g)	Mesopores volume (cm^3/g)	$\frac{MesoporesVolume}{TotalVolume}\times 100$ (%)
H200	63	50.1	12.9	0.288	0.006	0.282	97.9
H400	62.7	54.8	7.9	0.276	0.003	0.273	98.9
H600	60.5	48.9	11.6	0.306	0.005	0.301	98.4
H800	54	49.5	4.5	0.265	0.002	0.263	99.2
H1000	17.8	9.6	8.2	0.089	0.004	0.085	95.5

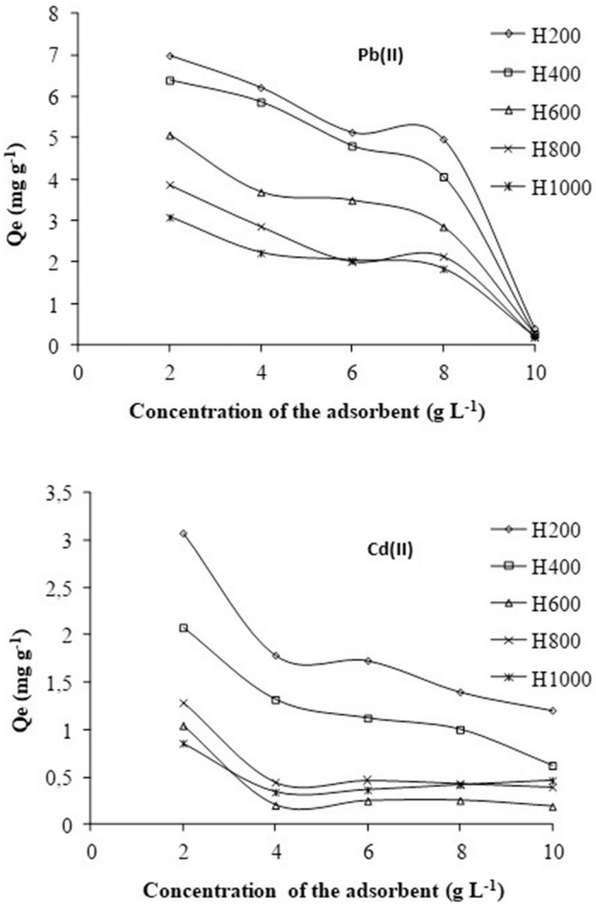

Fig. 4. Effect of solid/solution concentration on the amount adsorbed by the halloysite solids.

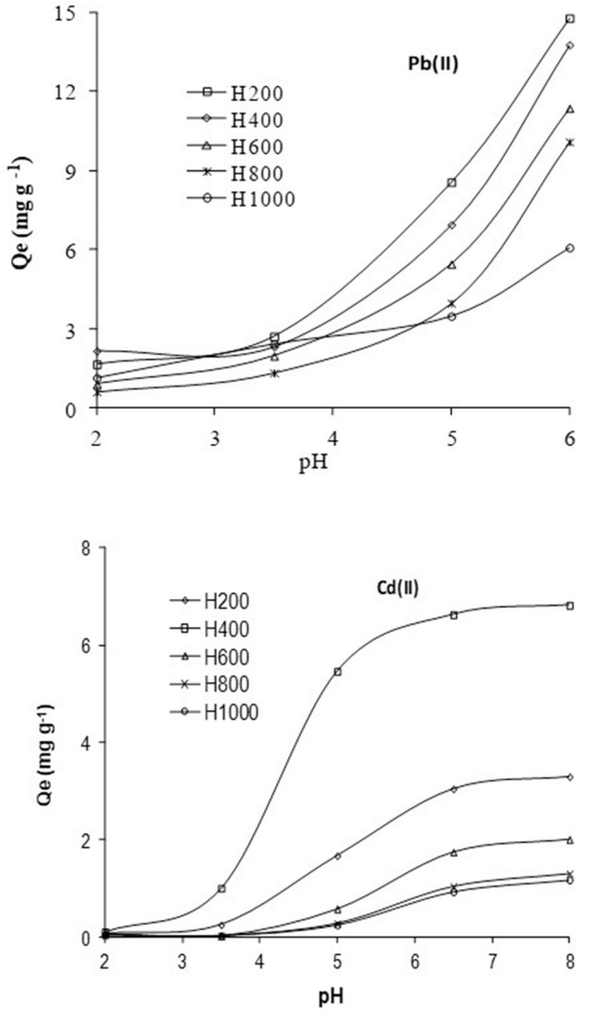

Fig. 5. Effect of pH on the adsorption of Cd(II) and Pb(II) onto the halloysite solids.

positively charged Pb(II) or Cd(II) species and negatively charged binding sites, owing to SO^- groups.

3.2.3. Effect of contact time

The effect of contact time on the adsorption of Cd(II) and Pb(II), at pH 6.0 and 6.5, respectively, was investigated in the range 1–120 min (Fig. 6). Adsorption rate is rapid in the first 10 min. This phenomenon could be attributed to the instantaneous occupancy of the most readily available sites on the adsorbent surface. Thereafter, it decreases gradually, reaching equilibrium at about 1 h. Further increase in contact time did not change significantly heavy metal removal. So, an agitation time of 2 h seems to be sufficiently long to achieve equilibrium. Fast adsorption at the initial contact time is due to the availability of the negatively charged surface sites. From 30 min, a quasi-stationary state is obtained, in which the adsorbed amount is almost constant, and may be attributed to a very slow diffusion rate of metal through the adsorbent micropores [33]. As the volume of micropores is negligible for all halloysitic materials, uptake is insignificant between 30 and 60 min. The parameters corresponding to the employed kinetic models are reported in Table 3. The pseudo-first-order equation was found unsuitable. Determination coefficients, R^2, are low, and the estimated theoretical quantities, $Q_{e(cal)}$, are different from the experimental values, $Q_{e(exp)}$. The fit of the experimental data with the pseudo-second-order model is more appropriate. Linear plots of t/Q vs. t [Eq. (2)] were obtained (data not shown), corresponding to high R^2 values, i.e., > 0.99. The $Q_{e(cal)}$ and $Q_{e(exp)}$ values are in close agreement (Table 3). This model was successfully applied for the bioadsorption of Cd and Pb by lignocellulosic biomass [30]. Contrary to the other models, the second-order equation predicts adsorption behavior over the entire investigated range, for which both metal cations and adsorbent really take part. Except for H400, initial rates, h, are higher for lead adsorption. As hydration energies of Pb(II) and Cd(II) are 1481 and 1807 kJ mol^{-1}, respectively [34], cadmium cations strongly maintain their hydration shell and, then, diffuse slowly in the halloysitic matrix. The evolution of rate constants, $K_{2,}$

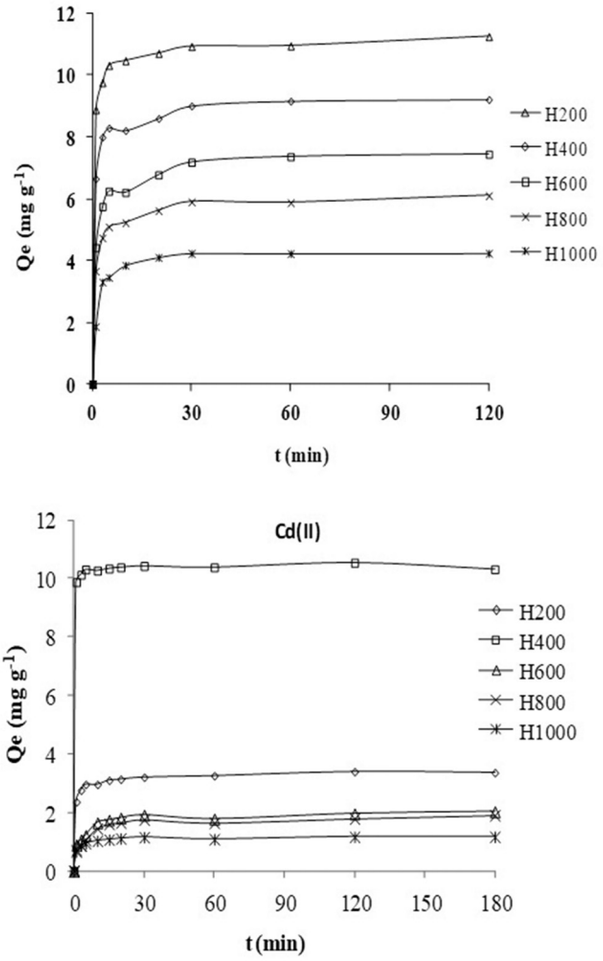

Fig. 6. Effect of contact time on the adsorption of Cd(II) and Pb(II) onto the halloysite solids.

with initial rates is not clear, indicating that the adsorption of heavy metals onto modified halloysites does not follow only the kinetics of second-order. The possibility of the intraparticle pore diffusion of adsorbate is always present. The plots of Q_t vs. $t^{1/2}$ [Eq. (4)] led to three linear portions (figures not shown). The first represents the external transport of mass, the second, intraparticle diffusion, and the last, surface saturation [19]. High R^2 values ($\geq$ 0.99) were obtained (Table 3), corresponding to the second linear portion. The values of intraparticle diffusion rate, K_{id}, are higher for Pb adsorption. As the hydration energy of lead is weaker, it would be easy for these cations to diffuse into the pores of the adsorbents. The values of intercept, *C*, give an idea about the thickness of boundary layer, i.e., the larger intercept, the greater is the boundary layer effect [35]. Overall, the parameter *C* decreases with increasing temperature. Thermal treatment disrupts the interfacial properties of our materials, so that the external mass transport across boundary layer affects the adsorption of cadmium and lead to some extent.

3.2.4. Adsorption equilibrium

3.2.4.1. Isotherms

Adsorption equilibrium was studied via a bath process at 25, 40, and 50°C. The isotherms are depicted in Figs. 7 and 8. Using the classification of Giles et al. [36], the obtained isotherms are L-shaped. The initial curvature of L-curve shows that pollutants have a high affinity for surface, while the slope falls steadily with a rise in concentration. The isotherms of Pb(II) (Fig. 7) indicates that the adsorbed amount decreases from 25 to 40°C, and then increases at 50°C for all materials. However, maximum adsorption occurs at 25°C. These results show that adsorption is exothermic in the range 25–40°C, and thereafter becomes endothermic. The increase in lead uptake from 40 to 50°C may be attributed to either an increase in number of available active surface sites or increase in the mobility of Pb(II) cations [37]. Zhou et al. [38] also reported a similar behavior for the removal of Pb(II) by modified cellulose, i.e., maximum capacity at 30°C, followed by a decrease at 50°C. Adsorption of Cd(II) (Fig. 8) decreases with increasing temperature on the interval of temperatures studied, indicating that low temperature favors cadmium removal from aqueous solution, and suggesting physical process.

3.2.4.2. Affinity

Maximum uptakes for each material towards lead and cadmium are reported in Table 4. Affinity follows the following sequences: H200 > H400 > H800 > H600 > H1000 for lead, and H400 > H200 > H600 > H800 > H1000 for cadmium. This trend is valid for any temperature. The maximum amounts of Pb(II) and Cd(II) adsorbed were 27.34 and 20.06 mg g^{-1}, respectively. Whatever heavy metal, maximum adsorption occurs for the material that preserves its structure. As revealed from XRD, the crystalline structure of halloysite is stable until 400°C. For H600 and H800, poorly organized structures with progressive amorphisation develop. So, the diffusion of Pb(II) and Cd(II) into halloysite matrix is prevented by the absence of a well-ordered porosity. Another reason must be invoked: H600 and H800 undergo dehydroxylation, while the adsorption of Pb(II) and Cd(II) mainly involves an electrostatic interaction between these metallic cations and the hydroxyl groups of surface, as suggested by the pH study. The lowest affinity showed by H1000 would be explained by its specific surface: 17.8 m^2 g^{-1} compared to approximately 60 m^2 g^{-1} for the remaining samples.

The following order was obtained for metal adsorption: Pb(II) > Cd(II), regardless of studied sample. We observed this trend even when the data were plotted as Q_e (mmol g^{-1}) against C_e (mmol L^{-1}) (figures not shown). This evolution must be correlated with their ionic properties, i.e., ionic radius, electronegativity, hydration energy, and ionic potential. As hydration energies of Pb(II) and Cd(II) are 1481 and 1807 kJ mol^{-1}, respectively, Pb(II) ions lose their hydration shell more easily and, thus, have a larger access to surface sites of halloysitic clays. In addition, the better affinity of Pb(II) might be also attributed to its higher electronegativity and ionic potential. This indicates that Pb(II) cations interact more strongly electrostatically

Table 3
Kinetic parameters for the Cd(II) and Pb(II) adsorption onto the halloysite solids

	Samples	Pseudo-first order model				Pseudo-second order model				Intraparticle diffusion model		
		Q_e (exp) (mg g^{-1})	K_1 (min^{-1})	Q_e (cal) (mg g^{-1})	R^2	Q_e (cal) (mg g^{-1})	K_2 (g mg^{-1} min^{-1})	h (mg g^{-1} min^{-1})	R^2	K^{id} (mg g^{-1} min$^{-1/2}$)	C (mg g^{-1})	R^2
Pb(II)	H200	11.252	0.0059	1.330	0.7290	11.26	0.1236	15.65	0.9998	0.1991	9.83	0.9943
	H400	9.210	0.0114	1.726	0.9522	9.27	0.1303	11.15	0.9999	0.3413	7.11	0.9924
	H600	7.441	0.0108	2.093	0.9540	7.52	0.0982	5.54	0.9998	0.4215	4.87	0.9997
	H800	6.097	0.0072	1.364	0.7441	6.13	0.1242	4.62	0.9997	0.2911	4.30	0.9998
	H1000	4.111	0.0025	1.732	0.4099	4.15	0.4120	6.96	0.9998	0.1702	3.31	0.9867
Cd(II)	H200	3.394	0.0385	0.845	0.5856	3.39	0.2768	3.19	0.9996	0.0654	2.84	0.9996
	H400	10.540	0.0387	0.667	0.2905	10.53	0.4681	50.75	1	0.0545	10.13	0.9905
	H600	2.305	0.0421	0.712	0.4683	1.96	0.2228	0.86	0.9969	0.1067	1.32	0.9967
	H800	1.787	0.0475	0.709	0.4963	1.80	0.2591	0.84	0.9963	0.0957	1.23	0.9902
	H1000	1.165	0.0426	0.296	0.4129	1.16	0.7996	1.08	0.9989	0.0503	0.88	0.9906

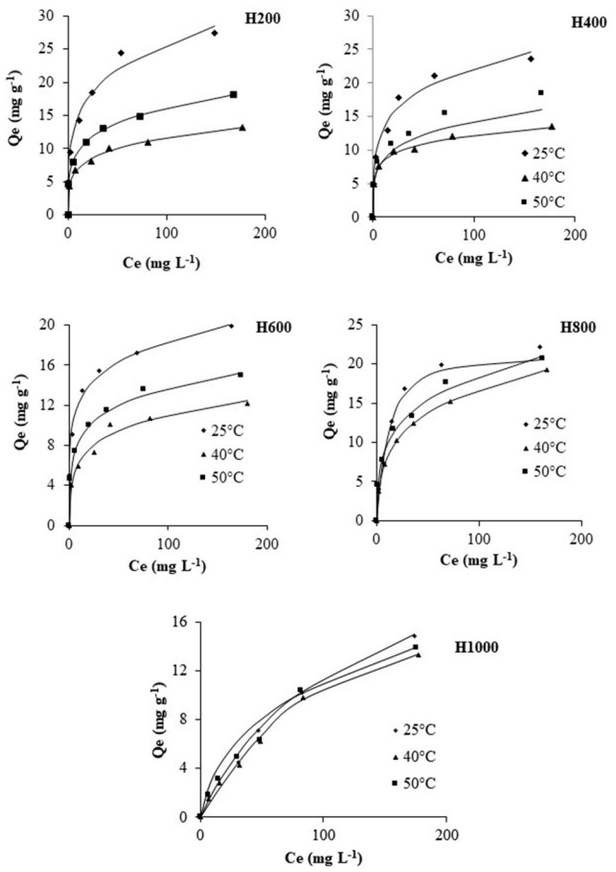

Fig. 7. Adsorption isotherms of Pb(II), according to the experimental data (…) and RP model, (—), onto the halloysite solids.

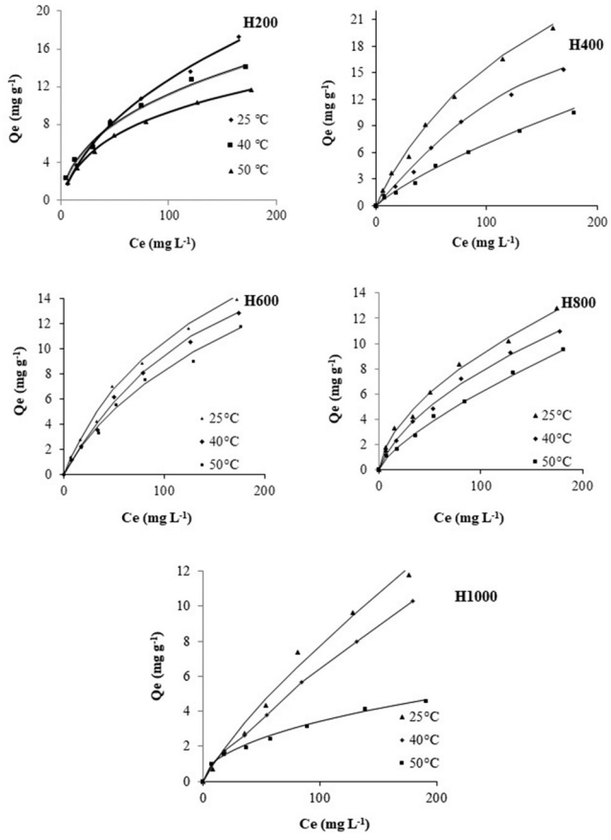

Fig. 8. Adsorption isotherms of Cd(II), according to the experimental data (…) and RP model, (—), onto the halloysite solids.

Table 4
Maximum uptake and ionic properties of Cd(II) and Pb(II)

Materials	Maximum uptake and ionic properties of Cd(II)			Maximum uptake and ionic properties of Pb(II)		
	Q_{max} (mg g^{-1})	Hydrated ionic radius (Å)	Hydration energy (kJ mol^{-1})	Q_{max} (mg g^{-1})	Hydrated ionic radius (Å)	Hydration energy (kJ mol^{-1})
H200	17.30			27.34		
H400	20.06			23.58		
H600	13.94	4.26	1807	19.90	4.01	1481
H800	12.77			22.19		
H1000	11.76			14.81		

with the groups present on the adsorbent surface [33]. In this sense, the hydrated ionic radius of Cd(II) (4.26 Å), compared to that of Pb(II) (4.01 Å), implies a fast saturation of adsorption sites, owing to steric hindrance. Surface available for hydrated Pb(II) is then greater than that for Cd(II) [39].

3.2.4.3. Fitting the models to the experimental data

Fitting of adsorption isotherm equations to experimental data is an important aspect of data analysis. The accuracy of model fit to experimental data is given by the determination coefficient, R^2, which is the square of the correlation coefficient, R, and the average relative error, E%. The parameters of Langmuir, Freundlich, and Redlich–Peterson models are gathered in Table 5. The Langmuir isotherm (Eq. (5) shows an inadequate fit of the experimental data. For Pb (II), average relative errors much higher than 10% were obtained, while R^2 values < 0.98 were found for almost all samples in relation to Cd (II). The low representativeness of this model with respect to the experimental data can be explained from its hypotheses: an adsorbent where all sites are identical and energetically equivalent seems to be unlikely for heat-treated halloysites. However, the Langmuir equation showed a good fit for Pb(II) and Cd(II) adsorption onto Australian zeolite [40]. The Freundlich equation [Eq. (6)] provides a satisfactory description of our experimental isotherms. The R^2 values are > 0.98, though some average relative errors are > 15%. Its validity indicates that adsorption takes place onto energetically heterogeneous solids. The Freundlich parameter K_F is appreciable for Pb(II) adsorption, in close agreement with its stronger retention. The exponent $1/n$ is less than unity for all adsorbents, implying that higher adsorption affinity occurs at lower concentrations. This model was found to be suitable for Pb(II), Cu(II), and Zn(II) adsorption onto kaolin [41]. Freundlich isotherm unfortunately fails at high concentration, because it does not have a finite saturation limit, and cannot be applied over a wide range of concentration.

The Redlich–Peterson model was used for the mathematical description of lead and cadmium isotherms. This equation includes three adjustable parameters and requires nonlinear regression. Its parameters were calculated and tabulated in Table 5. The Redlich–Peterson equation provides the best fit of the experimental isotherms. R^2 values are larger than 0.98, while those of E do not exceed 10%. This equation has a linear dependence on concentration in the numerator and an exponential function in the denominator, which intended it for both homogeneous and heterogeneous systems, and high concentrations. The RP model was successfully used for Cu(II) adsorption onto acetate-intercalated halloysites [29] and Cu(II), Cd(II), and Pb(II) onto activated carbon prepared from olive stones [42]. The values of β exponent are globally < 1, indicating favorable adsorption onto heterogeneous materials. The heterogeneity factor, β, depends on surface properties. Thermal activation results in deep changes in structure, texture, morphology, and surface reactivity with obtaining of energetically variable active sites.

3.2.5. Comparison with other adsorbents

The values of the maximum adsorption capacity of different adsorbents towards Pb(II) and Cd(II) are listed in Table 6. The results show that H200 and H400 have interesting capacities because higher than those of kaolinite, sawdust, and other biosorbents. Halloysite heated between 200 and 400°C appears very effective for removing heavy metals from wastewaters.

3.2.6. Thermodynamic parameters

The thermodynamic parameters obtained from Eqs. (8)–(10) are listed in Table 7. The overall negative values of $\Delta H°$ indicate that heavy metal adsorption is exothermic and an increase in temperature disadvantages process. The negative values of $\Delta S°$ suggest adsorbate–adsorbent systems much more ordered, for which the number of freedom degrees at the solid–liquid interface decreases with adsorption. Since stability is associated with an ordered arrangement, our metallic cations are in much more chaotic distribution in aqueous solution than in adsorbed state [48]. The positive values of $\Delta G°$ suggest a nonspontaneous process. However, Gibbs energy increases with increasing temperature, indicating that better adsorption is obtained at low temperature. In this context, when positive values of $\Delta G°$ are associated with negative values of $\Delta H°$ and $\Delta S°$, adsorption would be spontaneous at low temperature [49]. Ozdes et al. [50] also reported the spontaneous character of lead and cadmium adsorption onto illitic clay.

Table 5
Adjustable parameters of the Langmuir, Freundlich, and Redlich–Peterson models

	Samples		Langmuir					Freundlich				Redlich–Peterson				
		T (K)	Q_e(exp) (mg g^{-1})	Q_m (mg g^{-1})	K_L (L mg^{-1})	R^2	E (%)	K_F (L g^{-1})	n	R^2	E (%)	M (mg g^{-1})	β	K_{RP} (L mg^{-1})	R^2	E (%)
Pb(II)	H200	298	27.34	28.49	0.130	0.993	25.89	7.383	3.606	0.992	4.43	3.952	0.758	23.800	0.979	4.75
		313	15.61	13.70	0.087	0.989	10.59	4.121	4.417	0.994	2.48	1.989	0.783	34.318	0.993	2.15
		323	18.78	21.88	0.081	0.990	20.23	5.006	3.873	0.995	2.92	3.766	0.779	7.491	0.999	1.27
	H400	298	23.58	24.45	0.134	0.990	21.85	6.639	3.781	0.992	5.12	4.888	0.780	9.951	0.977	7.55
		313	13.48	13.76	0.138	0.995	22.34	5.852	6.250	0.994	2.18	1.561	0.838	3358.7	0.991	2.23
		323	18.46	19.12	0.092	0.986	25.50	5.745	4.462	0.996	2.45	0.943	0.766	1908.9	0.995	2.85
	H600	298	17.90	20.20	0.174	0.995	23.86	7.711	5.195	0.995	2.93	3.440	0.823	131.78	0.993	2.89
		313	12.13	12.76	0.086	0.994	13.59	3.318	3.931	0.995	4.48	3.901	0.798	1.820	0.976	6.07
		323	14.95	15.48	0.117	0.996	16.34	4.719	4.227	0.991	3.38	4.498	0.813	4.082	0.993	2.42
	H800	298	22.19	23.82	0.103	0.995	19.43	5.666	3.434	0.992	15.38	25.024	1.015	0.070	0.994	6.64
		313	19.61	20.49	0.059	0.994	13.82	3.353	2.827	0.992	4.20	5.564	0.746	0.870	0.997	2.86
		323	20.63	21.83	0.077	0.996	17.97	4.550	3.241	0.992	4.04	3.993	0.742	4.010	0.990	4.32
	1000	298	14.81	23.04	0.010	0.993	27.47	0.494	0.873	0.992	30.54	22.913	0.910	0.010	0.995	8.02
		313	13.29	21.51	0.009	0.962	6.96	0.497	2.221	0.990	6.85	26.398	1.456	0.006	0.995	9.48
		323	13.88	20.33	0.012	0.943	12.06	0.568	1.587	0.992	4.15	6.390	0.685	0.103	0.992	9.51
Cd(II)	H200	298	17.30	26.04	0.010	0.972	4.23	0.583	1.484	0.991	5.84	7.662	0.575	0.067	0.997	3.11
		313	13.98	17.57	0.020	0.969	8.50	1.024	1.926	0.990	5.67	3.776	0.618	0.243	0.992	4.74
		323	11.69	1.47	0.195	0.988	4.37	1.296	1.849	0.990	4.65	7.004	0.725	0.065	0.999	1.77
	H400	298	20.06	37.31	0.007	0.942	4.92	0.454	1.313	0.992	6.61	38.515	0.926	0.007	0.997	5.56
		313	15.36	41.49	0.020	0.969	6.34	0.215	1.182	0.990	8.23	34.778	1.703	0.004	0.996	7.10
		323	10.39	30.67	0.030	0.779	5.61	0.129	1.171	0.991	7.44	15.134	0.442	0.009	0.999	7.40
	H600	298	13.94	23.70	0.008	0.950	5.28	0.358	1.376	0.990	6.61	22.624	0.875	0.009	0.994	5.60
		313	12.88	26.95	0.005	0.923	4.97	0.277	1.250	0.990	7.37	27.493	1.182	0.005	0.995	4.46
		323	11.74	20.88	0.007	0.907	6.07	0.259	1.344	0.990	7.17	17.756	0.774	0.009	0.989	6.87
	H800	298	12.77	17.33	0.013	0.925	10.25	0.606	1.700	0.992	5.04	0.163	0.437	13.784	0.993	4.33
		313	10.97	16.81	0.010	0.930	4.97	0.390	1.543	0.996	3.61	4.717	0.531	0.059	0.996	4.96
		323	9.48	17.24	0.060	0.848	5.99	0.277	1.399	0.991	5.49	0.104	0.309	4.507	0.997	5.99
	1000	298	11.76	51.28	0.005	0.574	7.08	0.108	1.080	0.991	7.35	14.422	0.391	0.011	0.988	9.88
		313	10.30	20.28	0.005	0.825	9.49	0.199	1.318	0.991	4.68	11.102	0.366	0.012	0.998	7.03
		323	4.55	5.77	0.016	0.944	10.13	0.359	2.075	0.991	4.23	0.332	0.540	1.726	0.990	5.55

Table 6
Comparison of uptake capacities of Cd(II) and Pb(II) for various adsorbents

Adsorbent	Q_m (mg/g); [Ref.] Cd	Adsorbent	Q_m (mg/g); [Ref.] Pb
Natural kaolinite	0.88; [43]	Natural kaolinite	2.35; [43]
Rice husk	8.58; [44]	Rice husk	8.60; [44]
Sawdust of Populus alba	8.88; [45]	Sawdust of Populus alba	10.13; [45]
Neem oil cake	11.82; [46]	Watermelon seed hulls	24.15; [47]
H400	20.06	H200	27.34

Table 7
Thermodynamic parameters for the Cd(II) and Pb(II) adsorption onto halloysite solids

Samples	Pb(II)					Cd(II)				
	$\Delta H°$ (kJ mol^{-1})	$\Delta S°$ (kJ mol^{-1} K^{-1})	$\Delta G°$ (kJ mol^{-1})			$\Delta H°$ (kJ mol^{-1})	$\Delta S°$ (kJ mol^{-1} K^{-1})	$\Delta G°$ (kJ mol^{-1})		
			298 K	313 K	323 K			298K	213K	223K
H200	–26.10	–0.088	0.094	1.413	2.292	–7.093	–0.037	3.898	4.451	4.82
H400	–16.30	–0.056	0.484	1.329	1.892	–3.114	–0.118	4.106	5.88	7.063
H600	–26.50	–0.091	0.532	1.892	2.799	–9.377	–0.049	5.119	5.849	6.336
H800	–22.84	–0.093	4.852	6.245	7.173	–16.495	–0.072	4.951	6.03	6.75
H1000	2.57	–0.008	4.883	4.999	5.076	–30.474	–0.124	6.409	8.266	9.504

3.2.7. FTIR analysis and adsorption mechanism

The infrared spectra of H200 and Pb-loaded H200 (H200 after adsorption of Pb(II)) were recorded in the 4000–400 cm^{-1} range and depicted in Fig. 9. We considered only Pb-loaded H200 because cadmium interacts with the halloysite framework in the same way as lead.

The FTIR spectrum of H200 shows two bands at 3697 and 3621 cm^{-1} attributed to the stretching vibrations of the inner-surface and inner sheet hydroxyls, respectively [51]. The 1090 and 1036 cm^{-1} bands were assigned to the stretching modes of apical Si–O and Si–O–Si, respectively [52]. The band at 469 cm^{-1} was attributed to the Si-O-Si bending.

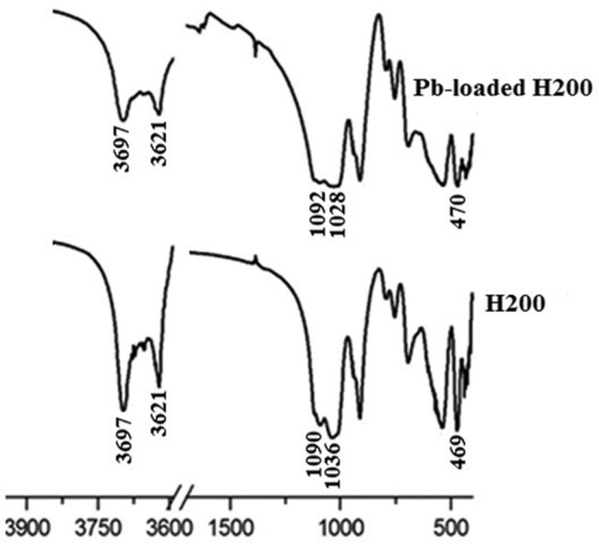

Fig. 9. FTIR spectra of H200 and Pb-loaded H200.

After lead adsorption, the intensity of the 3697 and 3621 cm^{-1} bands decreases, indicating the deep involvement of hydroxyl groups in the adsorption of heavy metals. Goyne et al. [53] showed that the proton dissociation on silanol surface sites starts at circumneutral pH as follows:

$$\equiv SiOH + OH^- \leftrightarrow \equiv SiO^- + H_2O \quad (15)$$

Bearing in mind that the adsorption of Pb cations (or Cd(II)) was performed at pH 6–6.5, attractive electrostatic interactions occur between the negatively charged sites of the H200 material and M^{2+} (M= Pb or Cd) cations. Such an interaction is justified by the slight change in the shape and position of the peaks of Pb-loaded H200.

4. Conclusion

Thermal treatment of Algerian halloysite from 200 to 1000°C resulted in significant changes in structure, texture, morphology, and surface reactivity. The crystal structure of halloysite has been preserved up to 400°C. Dehydroxylation occurred between 480 and 640°C, while a recrystallization process took place at ca. 1000°C, leading to the formation of γ-Al_2O_3. These materials were tested for removing Cd(II) and Pb(II) from aqueous solution. The adsorption of these metal cations was pH-dependent, spontaneous at low

temperature, and exothermic in nature. The kinetic and equilibrium data were adequately described by the pseudo-second order and Redlich–Peterson models, respectively. Maximum adsorption capacity was found to be 27.34 and 20.06 mg g^{-1} for Pb(II) and Cd(II), respectively, and was linked to samples that preserved their structure. A well-ordered porosity facilitates the diffusion of Pb and Cd cations into the halloysite lattice. The adsorption of heavy metals is governed by the electrostatic attraction between positively charged cations and negatively charged adsorption sites. The preferential adsorption of Pb compared to Cd was explained through their ionic properties, i.e. ionic radius, electronegativity, and hydration energy. The novelty of this paper is that a thermally activated halloysite, without structure destruction, can be effectively used as a low-cost and sustainable adsorbent for removing toxic metals from aqueous solutions.

Supplementary data available

Fig. S1 presents XRD patterns of unheated and halloysites heated at 200, 400, 600, 800, and 1000°C.

References

[1] R.T. Wilkin, Monitored natural attenuation of inorganic contaminants in ground water. Assessment for non-radionuclides including arsenic, cadmium, chromium, copper, lead, nickel, nitrate, perchlorate, and selenium. EPA 600/R-07/140. U.S. Environmental Protection Agency, Washington, DC, 2 (2007).
[2] H.K. An, B.Y. Park, D.S. Kim, Crab shell for the removal of heavy metals from aqueous solution, Water Res., 35 (2001) 3551–3556.
[3] A. Rani, A. Kumar, A. Lal, M. Pant, Cellular mechanisms of cadmium-induced toxicity: A review, Int. J. Environ. Health Res., 24 (2014) 378–399.
[4] P. Mitra, S. Sharma, P. Purohit, P. Sharma, Clinical and molecular aspects of lead toxicity: An update, Crit. Rev. Clin. Lab. Sci., 54 (2017) 506–528.
[5] K.G. Bhattacharyya, S. Sen Gupta, Adsorption of a few heavy metals on natural and modified kaolinite and montmorillonite, Adv. Colloid Interface Sci., 140 (2008) 114–131.
[6] C. Magnenet, S. Lakard, C.C. Buron, B. Lakard, Functionalization of organic membranes by polyelectrolyte multilayer assemblies: Application to the removal of copper ions from aqueous solutions, J. Colloid Interface Sci., 376 (2012) 202–208.
[7] R. Khani, S. Sobhani, M.H. Beyki, Highly selective and efficient removal of lead with magnetic nano-adsorbent: Multivariate optimization, isotherm and thermodynamic studies, J. Colloid Interface Sci., 466 (2016) 198–205.
[8] N.K. Akunwa, M.N. Muhammad, J.C. Akunna, Treatment of metal-contaminated wastewater: A comparison of low-cost biosorbents, J. Environ. Manage., 146 (2014) 517–523.
[9] S. Yao, J. Zhang, D. Shen, R. Xiao, S. Gu, M. Zhao, J. Liang, Removal of Pb (II) from water by the activated carbon modified by nitric acid under microwave heating, J. Colloid Interface Sci., 463 (2016) 118–127.
[10] X. Li, H. Zhou, W. Wu, S. Wei, Y. Xu, Y. Kuang, Studies of heavy metal ion adsorption on Chitosan/Sulfydryl-functionalized graphene oxide composites, J. Colloid Interface Sci., 448 (2015) 389–397.
[11] Z. Danková, A. Mockovčiaková, S. Dolinská, Influence of ultrasound irradiation on cadmium cations adsorption by montmorillonite, Desal. Water Treat., 52 (2014) 5462–5469.
[12] J. Hizal, P. Demirçivi, Ş. Karadirek, R. Apak, Investigation of individual and competitive adsorption of Cu (II), Cd (II), and Pb (II) on montmorillonite in terms of surface complexation and kinetic properties of Cu (II) adsorption, Desal. Water Treat., 57 (2016) 22441–22453.
[13] W.C. Tsai, S. Ibarra-Buscano, C.C. Kan, C.M. Futalan, M.L.P. Dalida, M.W. Wan, Removal of copper, nickel, lead, and zinc using chitosan-coated montmorillonite beads in single- and multi-metal system, Desal. Water Treat., 57 (2016) 9799–9812.
[14] S. Mellouk, S. Cherifi, M. Sassi, K. Marouf-Khelifa, A. Bengueddach, J. Schott, A. Khelifa, Intercalation of halloysite from Djebel Debagh (Algeria) and adsorption of copper ions, Appl. Clay Sci., 44 (2009) 230–236.
[15] S. Ziane, K. Marouf-Khelifa, H. Benmekki, J. Schott, A. Khelifa, Removal of a reactive textile azo dye by dolomitic solids: kinetic, equilibrium, thermodynamic, and FTIR studies, Desal. Water Treat., 56 (2015) 695–708.
[16] F. Bessaha, K. Marouf-Khelifa, I. Batonneau-Gener, A. Khelifa, Characterization and application of heat-treated and acid-leached halloysites in the removal of malachite green: Adsorption, desorption, and regeneration studies, Desal. Water Treat., 57 (2016) 14609–14621.
[17] S. Lagergren, Zur theorie der sogenannten adsorption gelöster stoffe (About the theory of so-called adsorption of soluble substances), K. Sven, Vetenskapsakad. Handl., 24 (1898) 1–39.
[18] Y.S. Ho, G. McKay, Pseudo-second order model for sorption processes, Process Biochem., 34 (1999) 451–465.
[19] W.J. Weber, J.C. Morris, Kinetics of adsorption on carbon from solution, J. Sanitary Eng. Div. Am. Soc. Civ. Eng., 89 (1963) 31–59.
[20] I. Langmuir, The adsorption of gases on plane surfaces of glass, mica and platinum, J. Am. Chem. Soc., 40 (1918) 1361–1403.
[21] H.M.F. Freundlich, Over the adsorption in solution, J. Phys. Chem., 57 (1906) 385–470.
[22] O. Redlich, D.L. Peterson, A useful adsorption isotherm, J. Phys. Chem., 63 (1959) 1024–1024.
[23] P. Yuan, P.D. Southon, Z. Liu, M.E.R. Green, J.M. Hook, S.J. Antill, C.J. Kepert, Functionalization of halloysite clay nanotubes by grafting with γ-aminopropyltriethoxysilane, Phys. Chem. C., 112 (2008) 15742–15751.
[24] G. Qiu, T. Jiang, G. Li, X. Fan, Z. Huang, Activation and removal of silicon in kaolinite by thermochemical process, Scand. J. Metall., 33 (2004) 121–128.
[25] M. Alkan, O. Demirbas, M. Dogan, Electrokinetic properties of kaolinite in mono- and multivalent electrolyte solutions, Microporous Mesoporous Mater., 83 (2005) 51–59.
[26] M. Kosmuski, E. Maczka, W. Janusz, J.B. Rosenholm, Multi-instrument study of the electrophoretic mobility of quartz, J. Colloid Interface Sci., 250 (2002) 99–103.
[27] K. Okada, H. Kawashima, Y. Saito, S. Hayashi, A. Yasumori, New preparation method for mesoporous γ-alumina by selective leaching of calcined kaolin minerals, J. Mater. Chem., 5 (1995) 1241–1244.
[28] Z. Rawajfih, N. Nsour, Thermodynamic analysis of sorption isotherms of chromium (VI) anionic species on reed biomass, J. Chem. Thermodyn., 40 (2008) 846–851.
[29] S. Mellouk, A. Belhakem, K. Marouf, J. Schott, A. Khelifa, Cu (II) adsorption by halloysites intercalated with sodium acetate J. Colloid Interface Sci., 360 (2011) 716–724.
[30] L.X. Zhong, X.W. Peng, D. Yang, R.C. Sun, Adsorption of heavy metals by a porous bioadsorbent from lignocellulosic biomass reconstructed in an ionic liquid, J. Agric. Food. Chem., 60 (2012) 5621–5628.
[31] K.O. Adebowale, I.E. Unuabonah, B.I. Olu-Owolabi, The effect of some operating variables on the adsorption of lead and cadmium ions on kaolinite clay, J. Hazard. Mater., 134 (2006) 130–139.
[32] A. Sari, M. Tuzen, D. Citak, M. Soylak, Equilibrium, kinetic and thermodynamic studies of adsorption of Pb (II) from aqueous solution onto Turkish kaolinite clay, J. Hazard. Mater., 149 (2007) 283–291.
[33] C. Lao, Z. Zeledon, X. Gamisans, M. Solé, Sorption of Cd (II) and Pb (II) from aqueous solutions by a low-rank coal (leonardite), Separ. Purif. Technol., 45 (2005) 79–85.

[34] E. Mobasherpour, M. Salahi, Pazouki, Comparative of the removal of Pb^{2+}, Cd^{2+}, and Ni^{2+} by nanocrystallite hydroxyapatite from aqueous solutions: Adsorption isotherm study. Arabian J. Chem., 5 (2012) 439–446.
[35] N.K. Kannan, M.M. Sundaram, Kinetics and mechanism of removal of methylene blue by adsorption on various carbons-A comparative study, Dyes Pigm., 51 (2001) 25–40.
[36] C.H. Giles, T.H. Mac Ewan, S.N. Nakhwa, D. Smith, Studies in adsorption. Part XI. A system of classification of solution adsorption isotherms, and its use in diagnosis of adsorption mechanisms and in measurement of specific surface areas of solids, J. Chem. Soc., 60 (1960) 3973–3993.
[37] J.C. Echeverria, I. Zarranz, J. Estella, J.J. Garrido, Simultaneous effect of pH, temperature, ionic strength, and initial concentration on the retention of lead on illite, Appl. Clay Sci., 30 (2005) 103–115.
[38] Y. Zhou, Q. Jin, X. Wang, B. Gao, M. Zhang, T. Ma, Removal of Pb (II) and malachite green from aqueous solution by modified cellulose, Cellulose, 21 (2014) 2797–2809.
[39] H. Benhima, M. Chiban, F. Sinan, P. Seta, M. Persin, Removal of lead and cadmium ions from aqueous solution by adsorption onto micro-particles of dry plants, Colloids Surfaces B: Biointerfaces, 61 (2008) 10–16.
[40] T.C. Nguyen, P. Loganathan, T.V. Nguyen, S. Vigneswaran, J. Kandasamy, R. Naidu, Simultaneous adsorption of Cd, Cr, Cu, Pb, and Zn by an iron-coated Australian zeolite in batch and fixed-bed column studies, Chem. Eng. J., 270 (2015) 393–404.
[41] X. Liu, P. Hicher, B. Muresan, N. Saiyouri, P.Y. Hicher, Heavy metal retention properties of kaolin and bentonite in a wide range of concentration and different pH conditions, Appl. Clay Sci., 119 (2016) 365–374.
[42] T. Bohli, A. Ouederni, N. Fiol, I. Villaescusa, Evaluation of an activated carbon from olive stones used as an adsorbent for heavy metal removal from aqueous phases, C.R. Chimie, 18 (2015) 88–99.
[43] M.Q. Jiang, X.Y. Jin, X.Q. Lu, Z.L. Chen, Adsorption of Pb (II), Cd (II), Ni (II), and Cu (II) onto natural kaolinite clay, Desalination, 252 (2010) 33–39.
[44] M.M.D. Zulkali, A.L. Ahmad, N.H. Norulakmal, O. Sativa, husk as heavy metal adsorbent: Optimization with lead as model solution, Bioresour. Technol., 97 (2006) 21–25.
[45] R. Najama, S. Muzaffar, A. Andrabi, Adsorption capability of sawdust of Populus alba for Pb (II), Zn (II), and Cd (II) ions from aqueous solution, Desal. Water Treat., 57 (2016) 29019–29035.
[46] R.A.K. Rao, M.A. Khan, Biosorption of bivalent metal ions from aqueous solution by an agricultural waste: Kinetics, thermodynamics and environmental effects, Colloids Surf., A., 332 (2009) 121–128.
[47] G. Akkaya, F. Guzel, Bioremoval and recovery of Cu (II) and Pb (II) from aqueous solution by a novel biosorbent watermelon (*Citrullus lanatus*) seed hulls: Kinetic study, equilibrium isotherm, SEM and FTIR analysis, Desal. Water Treat., 51 (2013) 7311–7322.
[48] S. Sen Gupta, K.G. Bhattacharyya, Immobilization of Pb (II), Cd (II), and Ni (II) ions on kaolinite montmorillonite surfaces from aqueous medium, J. Environ. Manage., 87 (2008) 46–58.
[49] W.L. Masterton, C.N. Hurley, Chemistry: Principles and Reactions, fifth ed., Brooks/Cole, California, CA, (2003).
[50] D. Ozdes, C. Duran, H.B. Senturk, Adsorptive removal of Cd (II) and Pb (II) ions from aqueous solutions by using Turkish illitic clay, J. Environ. Manage., 92 (2011) 3082–3090.
[51] N. Mahrez, S. Bendenia, K. Marouf-Khelifa, I. Batonneau-Gener, A. Khelifa, Improving of the adsorption capacity of halloysite nanotubes intercalated with dimethyl sulfoxide, Compos. Interfaces, 22 (2015) 403–417.
[52] Y. Deng, G.N. White, J.B. Dixon, Effect of structural stress on the intercalation rate of kaolinite, J. Colloid Interface Sci., 250 (2002) 379–393.
[53] K.W. Goyne, A.R. Zimmerman, B.L. Newalkar, S. Komarneni, S.L. Brantley, J. Chorover, Surface charge of variable porosity Al_2O_3(s) and SiO_2(s) adsorbents, J. Porous Mater., 9 (2002) 243–256.

Supplementary data

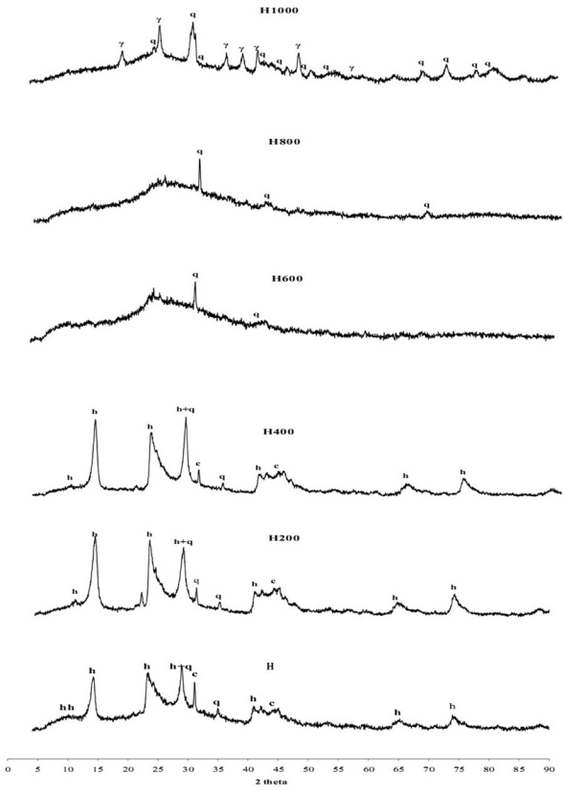

Fig. S1. XRD patterns of unheated and halloysites heated at 200, 400, 600, 800, and 1000°C.